Separation of Aero- and Vibroacoustic Noise from a Flexible Structure

J. Grabinger, S. Müller, S. Becker
Friedrich-Alexander University of Erlangen-Nuremberg, 91052 Erlangen, Germany,
Email: jens.grabinger@lse.eei.uni-erlangen.de

Introduction

The reduction of noise due to turbulent flow over a car's underbody is an important — yet complicated — issue in automotive engineering. Different structures in the underbody may generate noise by different mechanisms and of different spectral characteristics. Edges at struts of the underbody cause a turbulent flow, which usually radiates broad-band noise. On the contrary, metal sheets of the underbody are excited to vibration by the turbulent flow. The vibrations of the underbody typically contribute tonal components to the noise level, which correspond to its resonance frequencies. These two mechanisms of noise generation require different counter measures for noise reduction. Therefore it is desirable to identify the different types of noise in the spectrum of overall noise.

The objective of this paper is to separate the aeroacoustic and vibroacoustic contributions in the radiated sound. For this purpose we study the mechanisms of noise generation at a simplified model of a car's underbody. We mount a flexible rectangular plate into a rigid surrounding plate, which is then placed in a wind tunnel in parallel to the main flow direction. A square cylinder may be optionally mounted upstream of the flexible plate in order to model a strut. This setup generates noise by the same mechanisms as an underbody. We measure the sound pressure with a microphone and, simultaneously, the normal deflections of the plate with a laser scanning vibrometer. On the basis of these data we conduct FEM simulations in order to compute the vibrational sound at the position of the microphone. Subsequently, we estimate the contribution of the vibrational sound by comparing it to the measured data.

First the experimental setup is described. The next section will deal with the Finite Element scheme, that is used to conduct the simulation. After that the results of the experiments and the simulations will be discussed in detail.

Experiments

Mechanical Setup

The basis of the whole setup is a rigid plate (45 mm thick) made of aluminum, that is stiff enough not to vibrate itself. Inside this plate, a square hole with an edge of 150 mm length is cut out. The hole is then covered with a steel sheet of 40 µm thickness and an extent of 170 × 170 mm^2. It is glued to the underlying rigid plate at its edges on a margin of 10 mm. This results in an effective area of the flexible sheet of 150 × 150 mm^2. Next to that edge of the flexible plate, that will be facing upstream in the wind tunnel, a square cylinder with an edge length of 20 mm may be optionally mounted. We will conduct experiments both with and without the cylinder to study the quality of our approach under several flow conditions. The cylinder extends over the whole spanwise length of the rigid plate, so that its ends reach out of the wind tunnel's jet. This design ensures that the flexible plate is excited homogeneously over the whole of its span length. A schematic drawing of this assembly is shown in figure 1.

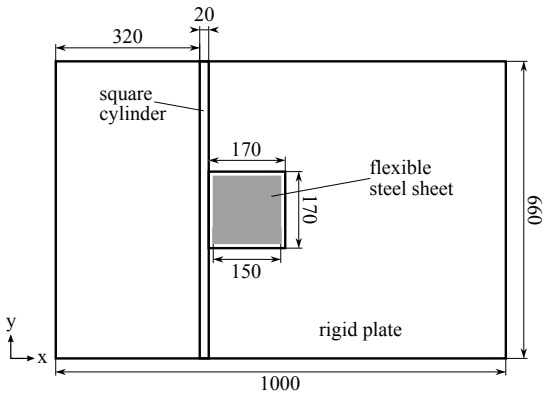

Figure 1: Sketch of the mechanical setup, front view (units in mm)

Measurements

The mechanical setup, that was described above, is mounted in the measuring section of an aeroacoustic wind tunnel in an anechoic room, as sketched in Figure 2. The upstream edge of the rigid plate is connected to the wind tunnel's nozzle. This results in a turbulent boundary layer over the rigid plate, that is influenced solely by the square cylinder (if present). There is a distance of 350 mm from the flexible plate to the wind tunnel's nozzle, in order to avoid interference of the vibrational sound with the wind tunnel's housing.

Measurements are conducted with and without the square cylinder at mean flow velocities of $\boldsymbol{v}_0 = 20\frac{\mathrm{m}}{\mathrm{s}}$ and $\boldsymbol{v}_0 = 40\frac{\mathrm{m}}{\mathrm{s}}$. The deflection of the flexible plate, that is caused by the turbulent flow, is measured with a laser scanning vibrometer. The scanning grid covers the whole flexible area (150 × 150 mm^2) of the steel sheet and consists of 31 × 31 points (5 mm spatial resolution). The measurement duration was chosen in such a way to achieve a frequency resolution of 1.25 Hz up to a cut-off frequency of 500 Hz.

Simultaneously, the sound pressure at a distance of 1 m

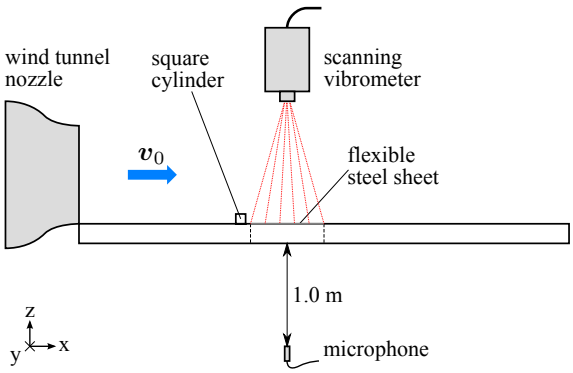

Figure 2: Sketch of the measurement setup, top view

behind the assembly (i.e. averted from the turbulent flow) is captured with a microphone. This is approximately the distance, where a car's driver would perceive the sound.

Finite Element Scheme

If only the first natural mode of the plate was excited, it would be sufficient to compute the correlation between the signals of the vibrometer and the microphone in order to identify the vibrational sound. But since we find that also higher modes are excited, this estimation is more complicated. Sound cancellation due to antiphased vibrational patterns have to be taken into account. Therefore a spatially resolved computation of the acoustic field is required. For this purpose we employ the Finite Element method. In order to compute the sound radiation from a vibrating structure numerically, we consider the partial differential equations of mechanical field and acoustic field, and the coupling condition at the interface of both fields.

Let us consider the deformation of a solid body $\Omega_s \subset \mathbb{R}^3$ with given density ρ_s and elasticity tensor $[\boldsymbol{c}]$. Assuming that the mechanical strain relates to the displacement $\boldsymbol{u}$ via the differential operator $\mathcal{B}$, the partial differential equation of linear elasticity reads

$$\rho_s \frac{\partial^2 \boldsymbol{u}}{\partial t^2} - \mathcal{B}^{\mathrm{T}}[\boldsymbol{c}]\mathcal{B}\boldsymbol{u} = 0. \tag{1}$$

The propagation of sound in a fluid domain $\Omega_f \subset \mathbb{R}^3$ with density ρ_f is described by the linear wave equation. Given the speed of sound c in the fluid, the partial differential equation for the acoustic velocity potential ψ reads

$$\frac{1}{c^2}\frac{\partial^2 \psi}{\partial t^2} - \boldsymbol{\Delta}\psi = 0. \tag{2}$$

Here ψ relates to the particle velocity fluctuations $\boldsymbol{v}'$ via

$$\boldsymbol{v}' = -\boldsymbol{\nabla}\psi. \tag{3}$$

In order to complete the problem formulation, the physical conditions at an interface between a solid and a fluid have to be modeled. Since the movement of the solid directly influences the movement of the fluid particles near the interface, a continuity condition (illustrated in Figure 3) can be set up. While the fluid particles can move freely in the direction tangential to the interface, the normal component of the acoustic particle velocity $\boldsymbol{v}'$ at the interface is dictated by the normal component of the mechanical surface velocity $\boldsymbol{v}_s$

$$\boldsymbol{n} \cdot \boldsymbol{v}' = \boldsymbol{n} \cdot \boldsymbol{v}_s, \tag{4}$$

where $\boldsymbol{n}$ denotes the surface normal vector at the solid-fluid interface pointing into the fluid domain. In terms of the variables of equations (1) and (2) this is equivalent to

$$-\boldsymbol{n} \cdot \boldsymbol{\nabla}\psi = \boldsymbol{n} \cdot \frac{\partial \boldsymbol{u}}{\partial t}. \tag{5}$$

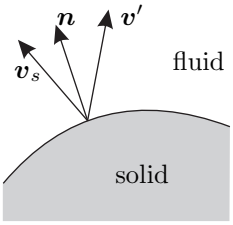

Figure 3: Continuity of the velocity at a solid-fluid interface

This condition is not sufficient though, because it does not take into account the influence of the fluid's movement on the solid. The pressure fluctuation p' of the ambient fluid causes a force $\boldsymbol{f}$ on the surface of the solid

$$\boldsymbol{f} = -\boldsymbol{n}p'. \tag{6}$$

Utilizing the relation $p' = \rho_f \partial\psi/\partial t$ [1] one can obtain the equivalent form

$$\boldsymbol{f} = -\rho_f \boldsymbol{n}\frac{\partial \psi}{\partial t}. \tag{7}$$

The weak formulation of the coupled field problem, that is required for applying the Finite Element Method, can be derived by multiplying equations (1) and (2) by appropriate test functions $\boldsymbol{w}, w$ and integrating over the fields' domains Ω_s, Ω_f. Subsequently Green's integral theorem is applied, so that the interface conditions (5) and (7) can be incorporated, which finally leads to

$$\int_{\Omega_s} \rho_s \boldsymbol{w} \cdot \frac{\partial^2 \boldsymbol{u}}{\partial t^2}\,\mathrm{d}\Omega + \int_{\Omega_s} (\mathcal{B}\boldsymbol{w})^{\mathrm{T}}[\boldsymbol{c}]\mathcal{B}\boldsymbol{u}\,\mathrm{d}\Omega + \int_{\Gamma} \rho_f \boldsymbol{w} \cdot \boldsymbol{n}\frac{\partial \psi}{\partial t}\,\mathrm{d}\Gamma = 0, \tag{8}$$

$$\int_{\Omega_f} \frac{1}{c^2} w \frac{\partial^2 \psi}{\partial t^2}\,\mathrm{d}\Omega + \int_{\Omega_f} \boldsymbol{\nabla} w \cdot \boldsymbol{\nabla}\psi\,\mathrm{d}\Omega - \int_{\Gamma} w\boldsymbol{n} \cdot \frac{\partial \boldsymbol{u}}{\partial t}\,\mathrm{d}\Gamma = 0, \tag{9}$$

where $\Gamma = \Omega_s \cap \Omega_f$ denotes the solid-fluid interface. It should be noted, that the boundary integrals differ in their sign due to the choice of the interface's normal vector $\boldsymbol{n}$. Additionally, this system of partial differential equations can be made symmetric by multiplying equation (9) by $-\rho_f$.

Next, the weak formulation of the problem is discretized using Galerkin's method, which yields a linear system of equations, that can be written in matrix form as

$$\begin{pmatrix} \mathbf{M}_u & 0 \\ 0 & \mathbf{M}_\psi \end{pmatrix} \begin{pmatrix} \underline{\ddot{u}} \\ \underline{\ddot{\psi}} \end{pmatrix} + \begin{pmatrix} 0 & \mathbf{C}_{u\psi} \\ \mathbf{C}_{u\psi}^{\mathrm{T}} & 0 \end{pmatrix} \begin{pmatrix} \underline{\dot{u}} \\ \underline{\dot{\psi}} \end{pmatrix} + \begin{pmatrix} \mathbf{K}_u & 0 \\ 0 & \mathbf{K}_\psi \end{pmatrix} \begin{pmatrix} \underline{u} \\ \underline{\psi} \end{pmatrix} = \begin{pmatrix} 0 \\ 0 \end{pmatrix}. \tag{10}$$

The coupling matrix $\mathbf{C}_{u\psi}$ is computed using the Mortar Finite Element Method [2], which allows for a non-conforming discretization of the solid-fluid interface.

It is important to note that the right hand side of the linear system is set to zero, because the excitation is prescribed in the z-component of the displacement u_z as an inhomogeneous Dirichlet boundary condition. u_z is determined as point-wise spectra of magnitude and phase by the measurements described above. Therefore, as a last step, the linear system of equations is transformed to the frequency domain [1]

$$\left(-\omega^2 \begin{pmatrix} \mathbf{M}_u & 0 \\ 0 & \mathbf{M}_\psi \end{pmatrix} + \omega \begin{pmatrix} 0 & \mathbf{C}_{u\psi} \\ \mathbf{C}_{u\psi}^{\mathrm{T}} & 0 \end{pmatrix} + \begin{pmatrix} \mathbf{K}_u & 0 \\ 0 & \mathbf{K}_\psi \end{pmatrix}\right) \begin{pmatrix} \underline{u} \\ \underline{\psi} \end{pmatrix} = \begin{pmatrix} 0 \\ 0 \end{pmatrix}, \tag{11}$$

where ω denotes the angular frequency. This formulation is more adequate than the time-domain formulation, as one can immediately obtain the time-harmonic solution in the whole computational domain. In order to achieve free field conditions, as given in the anechoic room, the Perfectly Matched Layers technique [3] is applied.

Results

The goal of our approach is to identify frequency bands in the spectrum of sound pressure level, that are dominated either by vibrational noise or by turbulence noise. The Finite Element method, that was presented above, provides us directly with a spectrum of the vibrational sound pressure. Computing the spectrum of the microphone signal is trivial, so that we can immediately proceed by comparing computed and measured sound pressure levels. First we will compare the spectra of the various flow conditions. After that we will take a closer look, why the sound radiation of the higher modes of the flexible plate can be estimated only numerically.

Let us consider the case without the square cylinder in front of the flexible plate at a mean flow velocity of 20 $\frac{\mathrm{m}}{\mathrm{s}}$. Both computed and measured spectra are shown in

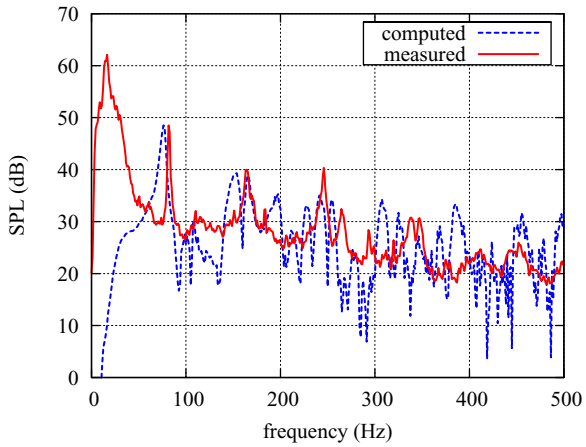

Figure 4: Comparison of computed and measured spectra of SPL (w/o square cylinder, $v_0 = 20\frac{\mathrm{m}}{\mathrm{s}}$)

Figure 4. One can immediately recognize the dominant peak in the measured spectrum at approx. 15 Hz, which is completely absent in the computed spectrum. This peak can be attributed to noise of the wind tunnel itself (see Figure 5), which obviously cannot be predicted using a vibroacoustic simulation. The second and third peaks in the measured spectrum are predicted very well by the simulation, even if the computed peaks are broader than the measured ones. The fourth peak in the measured spectrum is recognizable in the computed spectrum, too, although it is under-estimated by the simulation. Above 300 Hz no similarities between measurement and simulation can be found. The simulation result looks very noisy in this region, which may be due to noise in the vibrometer signal at low amplitudes. One can conclude that this configuration is dominated by vibrational sound.

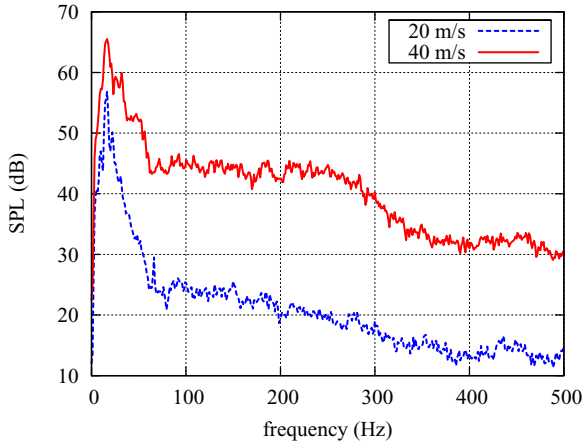

Figure 5: Measured SPL spectra of the empty measuring section of the aeroacoustic wind tunnel

A case, where both vibrational and flow-induced sound becomes relevant, is the configuration with square cylinder in front of the flexible plate at $v_0 = 20\frac{\mathrm{m}}{\mathrm{s}}$ (see Figure 6). The prediction of the first peak agrees very well with the measurement. Other relevant peaks are not predicted by the simulation. The other peaks in the measured spectrum can therefore be attributed to flow-

induced sound, generated by the turbulent flow around the square cylinder. Flow around cylinders is known to generate tonal sound [4].

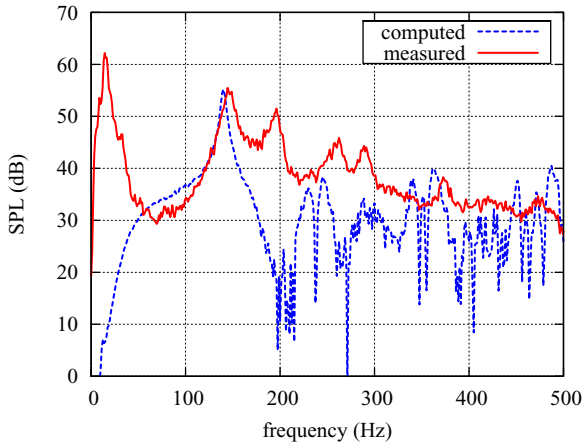

Figure 6: Comparison of computed and measured spectra of SPL (with square cylinder, $v_0 = 20\frac{\mathrm{m}}{\mathrm{s}}$)

The last configuration to be discussed here, is the same mechanical setup as the previous one, but at a mean flow velocity of 40 $\frac{\mathrm{m}}{\mathrm{s}}$. Again, the vibrational sound is dominant in the spectra shown in Figure 7. The measured spectrum follows the computed spectrum over almost the whole frequency range. The main deviation occurs below 250 Hz, which is due to broad-band sound of the turbulent boundary layer, and noise of the wind tunnel.

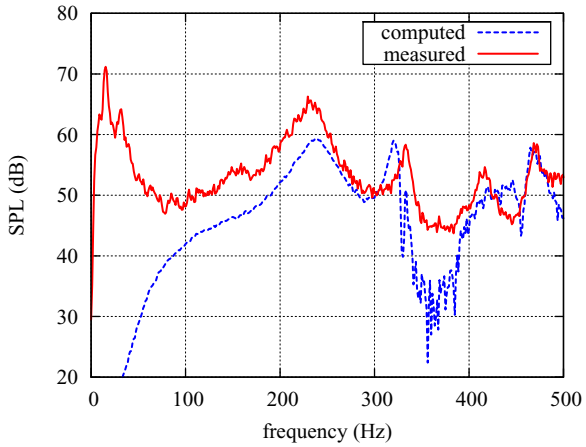

Figure 7: Comparison of computed and measured spectra of SPL (with square cylinder, $v_0 = 40\frac{\mathrm{m}}{\mathrm{s}}$)

Let us take a final look, why such a numerical simulation is required. Figure 8 shows the phase of the plate's vibrational pattern at 455 Hz, which correponds to the local minimum in the computed spectrum of SPL at 455 Hz, shown in Figure 7. One can easily identify the pattern of the third natural mode with an antiphased region in the center of the flexible plate. This results in a cancellation of sound pressure above the flexible plate (see Figure 9), which can be estimated correctly by a spatially resolved simulation only.

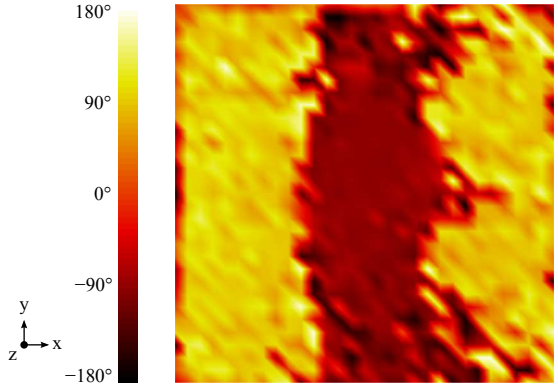

Figure 8: Phase of the flexible plate's displacement at 455 Hz (configuration with square cylinder, $v_0 = 40\frac{\mathrm{m}}{\mathrm{s}}$)

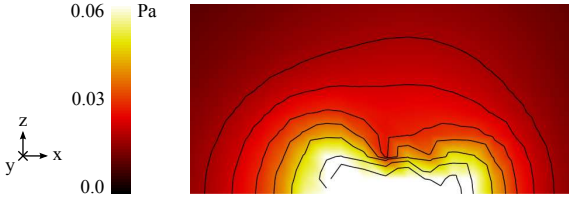

Figure 9: Sound cancellation due to antiphased vibration; sound pressure amplitude (in Pa) at 455 Hz in the central x-z plane above the flexible plate

Conclusions

The mechanisms of noise generation at a car's underbody were studied at a simplified experimental setup. FEM simulations of vibrational sound were conducted on the basis of measured deflection. This approach allows to separate vibrational noise and turbulence noise in the measured spectrum.

Acknowledgments

Funding by the Bavarian Research Foundation (Bayerische Forschungsstiftung, BFS) is gratefully acknowledged.

References

[1] Kaltenbacher, M.: Numerical Simulation of Mechatronic Sensors and Actuators. Springer-Verlag, Berlin Heidelberg New York, 2nd ed., 2007

[2] Flemisch, B., Kaltenbacher, M., Wohlmuth, B. I.: Elasto-acoustic and acoustic-acoustic coupling on non-matching grids. Int. J. Numerical Methods in Engineering **67** (2006), no. 13, 1791–1810

[3] Bermúdez, A., Hervella-Nieto, L., Prieto, A., Rodríguez, R.: An exact bounded PML for the Helmholtz equation. Comptes Rendus Mathematique **339** (2004), no. 11, 803–808

[4] Becker, S., Hahn, C., Kaltenbacher, M., Lerch, R.: Flow-Induced Sound of Wall-Mounted Cylinders with Different Geometries. AIAA Journal **46** (2008), no. 9, 2265–2281